electronic materials

MDPI

Article

Impedance Spectroscopy of Electrochromic Hydrous Tungsten Oxide Films

Esat Pehlivan [1,2], Claes G. Granqvist [1] and Gunnar A. Niklasson [1,*]

[1] Department of Materials Science and Engineering, The Ångström Laboratory, Uppsala University, P.O. Box 35, SE-75103 Uppsala, Sweden; esat.pehlivan@physics.uu.se (E.P.); claes-goran.granqvist@angstrom.uu.se (C.G.G.)
[2] ChromoGenics AB, Ullforsgatan 15, SE-75323 Uppsala, Sweden
* Correspondence: gunnar.niklasson@angstrom.uu.se

Abstract: Tungsten oxide is a widely used electrochromic material with important applications in variable-transmittance smart windows as well as in other optoelectronic devices. Here we report on electrochemical impedance spectroscopy applied to hydrous electrochromic tungsten oxide films in a wide range of applied potentials. The films were able to reversibly bleach and color upon electrochemical cycling. Interestingly, the bleaching potential was found to be significantly higher than in conventional non-hydrous tungsten oxide films. Impedance spectra at low potentials showed good agreement with anomalous diffusion models for ion transport in the films. At high potentials, where little ion intercalation takes place, it seems that parasitic side reactions influence the spectra. The potential dependence of the chemical capacitance, as well as the ion diffusion coefficient, were analyzed. The chemical capacitance is discussed in terms of the electron density of states in the films and evidence was found for a band tail extending below the conduction band edge.

Keywords: electrochromism; optoelectronic coatings; smart windows; hydrous tungsten oxide; impedance spectroscopy; chemical capacitance

Citation: Pehlivan, E.; Granqvist, C.G.; Niklasson, G.A. Impedance Spectroscopy of Electrochromic Hydrous Tungsten Oxide Films. *Electron. Mater.* **2021**, *2*, 312–323. https://doi.org/10.3390/electronicmat2030022

Received: 8 June 2021
Accepted: 21 July 2021
Published: 27 July 2021

1. Introduction

Electrochromic (EC) devices can reversibly change their optical properties when an external electrical potential is applied [1–3]. Their largest-scale technical application is in smart windows [4–6], which are available on the market since several years and able to impart energy efficiency and improved indoor comfort to buildings. Other important optoelectronic applications encompass various types of displays and sensors as well as rear-view mirrors for cars [2,5]. An EC device usually consists of a cathodic and an anodic EC coating separated by an electrolyte and sandwiched between transparent electrical contacts. Tungsten oxide (WO_3) is the most widely used cathodic EC material [5,7]. It exhibits significant optical absorption in the visible and near-infrared wavelength regions when intercalated by H^+ or Li^+ ions. Optical switching is intimately related to ion transport in the material, although it is the charge-compensating electrons—injected into the film from the transparent contact to preserve charge neutrality—that are responsible for the optical (polaronic) absorption [8]. Optical modulation in a device depends on the kinetics of ion intercalation in the cathodic and anodic materials as well as on the impedance of the electrolyte and the transparent conductor films. Hence, establishing the relation between optical and ion/electron transport properties constitutes a key issue in research on EC materials and devices.

Electrochemical impedance spectroscopy (EIS) is a powerful tool to characterize electrochemical reactions and ion intercalation systems [9,10]. In contrast with the commonly used voltametric, galvanostatic, and potentiostatic methods, it is a frequency-domain measurement rather than a time-domain measurement. The EIS technique has been frequently applied to EC materials and systems; a state-of-the-art review was presented recently [11]. EIS gives information about interfacial capacitance and charge transfer as well as on ion

diffusion coefficients and even, in some cases, on electronic density of states. In the pioneering work of Ho et al. [12], a so-called Randles equivalent circuit [13], including an ordinary diffusion element, was used to interpret experimental data. This model has been frequently used [14–18], but recently it has become apparent that there exist systematic discrepancies between experiments and the basic Randles model. Extensions to the model have involved effects of ion trapping [19,20] and anomalous diffusion phenomena [21]. In particular, anomalous diffusion models provide a versatile and accurate description of the frequency-dependent impedance of EC materials such as amorphous WO_3 [22,23] and polycrystalline IrO_2 [24]. As already remarked above, having information about diffusion kinetics is vital to controlling the kinetics of EC devices.

WO_3 is the most widely studied cathodic EC material. A detailed review focusing on sputter-deposited films of this material was given some years ago [7] and more recent developments can be found, for example, in [25–27]. Films sputtered at room temperature are known to be amorphous and crystallization does not start until temperatures above 400 K [28]. The review [7] included a few preliminary optical data on a seldom studied form of WO_3, produced by sputtering in a mixed Ar + O_2 + H_2 gas ambient. This thin-film deposition process was introduced by Giri and Messier [29] and yields films that are colored in as-deposited state. Hydrous WO_3 (denoted HWO_x below) has been used in EC devices together with dark as-prepared nickel oxide (NiO)-based anodic EC films [30,31]. A potential advantage of this device configuration is related to effects of stoichiometry on the electrochromism of NiO, since it has been shown that over-stoichiometric films (NiO_y with $y > 1$), which are strongly absorbing under as-deposited conditions, display a significantly larger optical modulation in commonly used Li^+-electrolytes than close-to-stoichiometric transparent films [32]. Absorbing NiO_y films must be combined with absorbing WO_3-based films in a device for the purpose of charge balancing between the anodic and cathodic films.

The discussion above points at the interest to study the EC properties of HWO_x films, but we are not aware of any previous detailed study of this kind. Here we present a thorough investigation of the variations in transmittance and impedance over a large potential range. Differences from conventional as-deposited transparent WO_3 films were observed, which may be of considerable significance for EC device applications. Furthermore, flexible polyester substrates—which are of major interest for applications [33], rather than glass substrates—were used in the present study. Section 2 below describes our experimental techniques, Section 3 gives a basic review of the theory of impedance response in EC materials, while Section 4 discusses our results in detail. Conclusions are given in Section 5.

2. Materials and Methods

Thin films of HWO_x were produced by reactive DC magnetron sputtering from a W target onto polyester substrates precoated with transparent and electrically conducting indium–tin oxide (ITO; sheet resistance 30 Ω/square). Sputtering was carried out using a power density of 3 W/cm^2 in an Ar + O_2 + H_2 atmosphere at a pressure of 3×10^{-2} mbar with a flow ratio of reactive gas to Ar of 0.3 and an O_2/H_2 flow ratio of 0.5. The luminous transmittance of the as-deposited films was about 40%; they exhibited a bluish color. The thickness of the films was ~300 nm, as inferred from surface profilometry. Detailed information about the sputtering process, as well as structural characterization of such films can be found elsewhere [29]. Films with active areas of 2×2 cm^2 were used in all experiments described below.

Electrochemical and optical measurements were carried out at applied potentials between 2.0 and 5.0 V vs. Li/Li^+ with intervals of 0.3 V. Fresh as-deposited films were used for the measurements at each applied potential. Electrochemical measurements on the HWO_x films were carried out in a MecaPlex CH-2540 glove box filled with Ar. The water content in the glove box was about 5 ppm. A three-electrode setup was used for the experiments with Li foils as reference and counter electrodes and HWO_x film as working electrode. The electrolyte was 1 M $LiClO_4$ dissolved in propylene carbonate. EIS measurements

were performed on a Solartron 1286 electrochemical interface together with a Solartron 1260 frequency response analyzer. An AC signal of 10 mV amplitude was superimposed on the applied DC potential. The frequency of the AC signal was scanned between 10^{-2} and 10^{5} Hz with ten data points per decade. Before starting each EIS measurement, the chosen DC potential was applied to the as-deposited film during a pretreatment period of 15 min to achieve a stable electrochemical state. The inserted or extracted charge at the chosen potential was obtained from this so-called chronoamperometry (CA) measurement by integrating the current recorded during the pretreatment period. The measurement procedure—encompassing pretreatment and ~35 min EIS measurement—was repeated four times at the same DC potential to assure that the data were reliable and reproducible.

After the electrochemical measurement requiring Ar atmosphere was completed, a constant potential was applied to the film for 10 min. Subsequently, the film was taken out of the glove box, cleaned by spraying with ethanol, and dried in a flow of nitrogen gas. Optical transmittance measurements on these films were carried out ex situ after coloration; data were recorded, at different potentials, in the 350–800-nm wavelength range using an Ocean Optics fiber-optic spectrometer.

3. Theory

Equivalent-circuit analysis is commonly used to analyze data from EIS measurements, such as those presented in detail below for EC HWO_x thin films. The impedance response is modeled by a circuit containing various circuit elements, which subsequently should be interpreted in terms of the electrochemical and electrical transport processes occurring in the sample under study. A variety of physical processes should be taken into consideration when formulating an equivalent-circuit model for WO_3-based films [11,23]: double-layer capacitance, charge transfer of ions from electrolyte to film, an intermediate adsorption step in which an ion combines with an electron from the conduction band of the film [34], ion diffusion in the film, as well as possible effects occurring at the back contact to the film. In some cases, constant-phase elements (CPEs) have to be used when fitting in order to describe the capacitive effects. A CPE has an impedance given by

$$Z_{CPE} = \left[\tau(i\omega)^n\right]^{-1}, \quad (1)$$

where τ is a generalized capacitance related to the amplitude of the CPE, ω is angular frequency, and n is a power-law exponent. It should be noted that an equivalent-circuit model is never unique, but in the present work we build on extensive previous experience of EIS studies of WO_3 thin films [11,22,23].

We first consider the potential region below 3.5 V vs. Li/Li^+ and employ a generalized Randles model, as in our previous works [22,23]. Figure 1a shows an equivalent circuit; it includes interfacial CPE and resistance elements as well as an anomalous diffusion element, which is used instead of the ordinary diffusion impedance. The interfacial elements may contain contributions from the electrochemical double-layer as well as from adsorption, since we were not able to separate these effects in our fits to experimental spectra. To describe anomalous diffusion, we use the "anomalous diffusion 1b" model from the work by Bisquert and Compte [21], which is based on a direct generalization of Fick's law to the case of fractional diffusion [35]. In Figure 1, R_{hf} is the high-frequency resistance due to the electrolyte and the ITO substrate, CPE_{int} is the constant-phase element describing the front (electrolyte/EC film) interface, R_{ct} is the effective charge transfer resistance (including adsorption effects) at the front interface, and Z_d is the diffusion impedance. The Z_d element describes diffusion in the film as well as back interface (EC film/ITO) effects, since diffusion is assumed to be blocked at the back interface. It is common to use a distributed element representation (generally a transmission line) for Z_d, as shown in the figure where q and c denote the impedance per unit length of the constant-phase element and the capacitance per unit length, respectively [21–23].

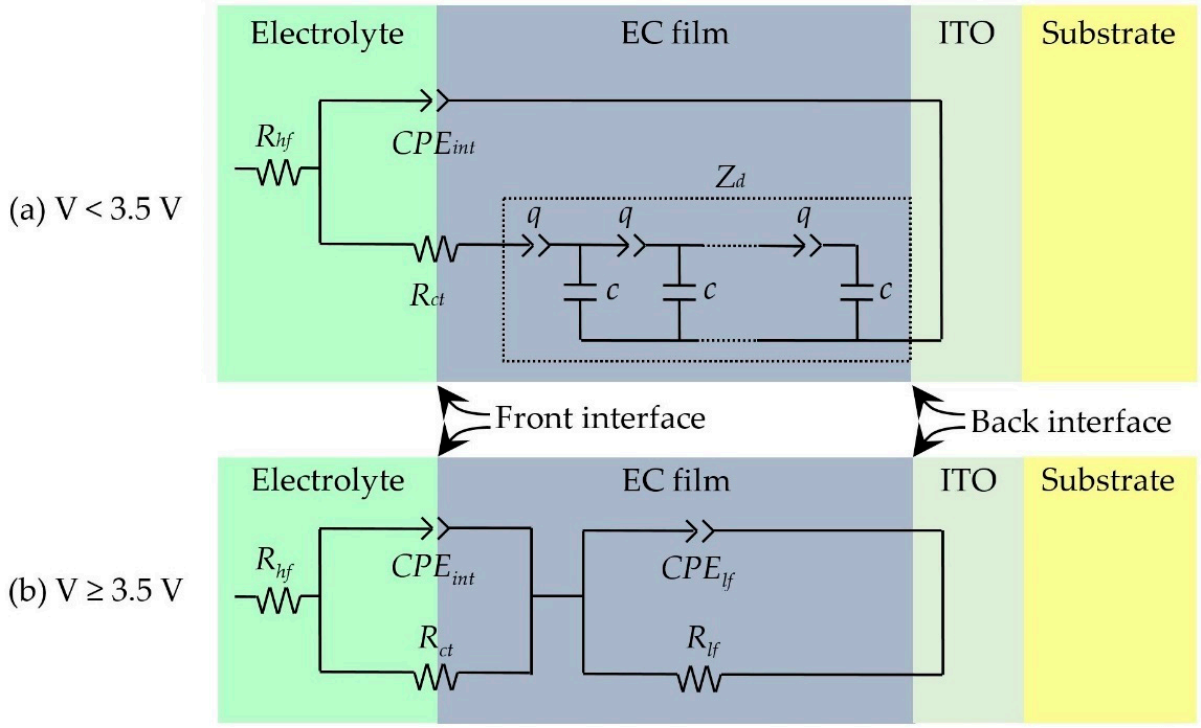

Figure 1. (**a**) Equivalent circuit used at potentials below 3.5 V vs. Li/Li^+ and constituent electrochemical system: an EC film immersed in an electrolyte. The rectangle within the bluish background delineates a transmission-line representation of the diffusion impedance Z_d for "anomalous diffusion 1b" (cf. main text). (**b**) Corresponding equivalent circuit used for potentials above 3.5 V vs. Li/Li^+.

The impedance of the depicted transmission line is given by [21]

$$Z_d(\omega) = R_\omega \omega_d^{\gamma-1} \left(\frac{\omega_d}{i\omega}\right)^{1-\frac{\gamma}{2}} \coth\left[\left(\frac{i\omega}{\omega_d}\right)^{\frac{\gamma}{2}}\right], \quad (2)$$

where $Z_d(\omega)$ is the diffusion impedance, R_ω is a pre-factor which only affects the magnitude of the impedance (the so-called "diffusion resistance"), ω_d is a characteristic frequency, and $\gamma = 1 - n_q$ is the power-law exponent of the CPE element q. This exponent can take values between 0 and 1.

At high potentials, above 3.5 V vs. Li/Li^+ where only little ion intercalation takes place, we were not able to obtain good fits to the generalized Randles circuit in Figure 1a. Instead, we replace the diffusion element with a second parallel R-CPE combination, as depicted in Figure 1b. Here R_{ct} and CPE_{int} have the same meaning as in Figure 1a, while the interpretation of the low-frequency parameters R_{lf} and CPE_{lf} is not obvious. The interpretation of these circuit elements may involve effects of the intermediate adsorption step [34] as well as of the impedance due to parasitic chemical reactions [10,36] in the system, which may occur at high potentials.

Equivalent-circuit fitting of experimental data was carried out by use of the software ZView [37]. Data points above frequencies of about 20 kHz were affected by parasitic effects such as those related to the counter and reference electrodes, as well as noise, and were excluded from the fits. In order to describe the quality of the fits, we use the weighted-sum-of-squares (WSSQ) deviation [37], in which the differences between experimental data and corresponding fit are weighted by the magnitude of the data values. This method has advantages when the fitted quantities vary by orders of magnitude, as is the case here.

From the anomalous diffusion element Z_d it is possible to determine the diffusion coefficient and the charge capacity of the films. The relation between the diffusion coefficient

D and the fitting parameters as well as the diffusion length L (in our case being the film thickness) is given by [22,24]

$$D = L^2\omega_d = L^2\left(c\tau_q^{-1}L^2\right)^{-1/\gamma}, \tag{3}$$

where τ_q denotes the capacitive amplitude of the CPE q in Figure 1a.

It is useful to know how much charge takes part in the electrochemical coloration/bleaching process of the HWO_x film. We can estimate how many ions per host atom are inserted when the applied potential, and therefore the energy, U, is changed. If z is defined as the number of inserted ions per host atom in the film, then

$$z = \frac{N_{ion}}{N_{host}} = \frac{Q_{ion}M}{eAd\rho N_A} \tag{4}$$

where Q_{ion} is the inserted/extracted ionic charge, which is equal to the electronic charge. In addition, M is the molar mass of the host material in which the ions are inserted, e is the charge of an electron, A is the active area of the film, d is the film thickness, ρ is the density of the film, and N_A is Avogadro's constant. The low-frequency chemical capacitance, C_{chem}, in an EIS measurement is given by [38]

$$C_{chem} = e^2\frac{dN}{dU} \tag{5}$$

where N is the number of electrons inserted together with the ions, and dN/dU is the number of electrons inserted per unit energy. The quantity dz/dU can now be found by using Equation (4). It has the appearance of an effective density-of-states and shows how many ions per host atom, or alternatively charge-compensating electrons, that are inserted in the film at a certain energy. This parameter gives a measure of the potential-dependent charge capacity and can give qualitative information about the electronic density of states in the film [39–41].

4. Results and Discussion

Figure 2 shows transmittance as a function of wavelength for a HWO_x film after electrochemical treatment at the given potentials. The potentials yield different coloration states with different amounts of ions intercalated into the film. The coloration/bleaching process is reversible and a continuous function of applied potential. It is seen that the optical contrast between colored and bleached states can be excellent and spans the range from 85% in the fully bleached state to below 10% in the fully colored state at mid-visible wavelengths. The transmittance spectra of as-deposited films were very close to the spectrum pertaining to 3.2 V vs. Li/Li^+, as seen in Figure 2.

We first discuss the charge corresponding to the fully bleached and dark states, obtained from the CA measurements. The bluish as-deposited HWO_x films could be fully bleached at 5.0 V vs. Li/Li^+, which required extracting a charge of 8.9 mC/cm^2. On the other hand, the dark state at 2.0 V vs. Li/Li^+ was reached by inserting a charge of 20.3 mC/cm^2 into an as-deposited film. Hence the total charge capacity was found to be 29.3 mC/cm^2, which is slightly higher than values reported for sputter deposited non-hydrous WO_3 films [27].

To assess the performance of the HWO_x films, we now consider the optical properties at a mid-luminous wavelength of 550 nm. At this wavelength, the transmittance contrast between fully bleached and dark states was about 0.72, corresponding to an optical density (OD) difference of 2.26. The coloration efficiency (CE) was obtained by dividing the OD difference by the charge inserted during coloration, starting at the bleached state. The obtained value of the CE, 77.2 cm^2/C, falls in the range of values for non-hydrous WO_3 films sputter deposited under similar conditions [27].

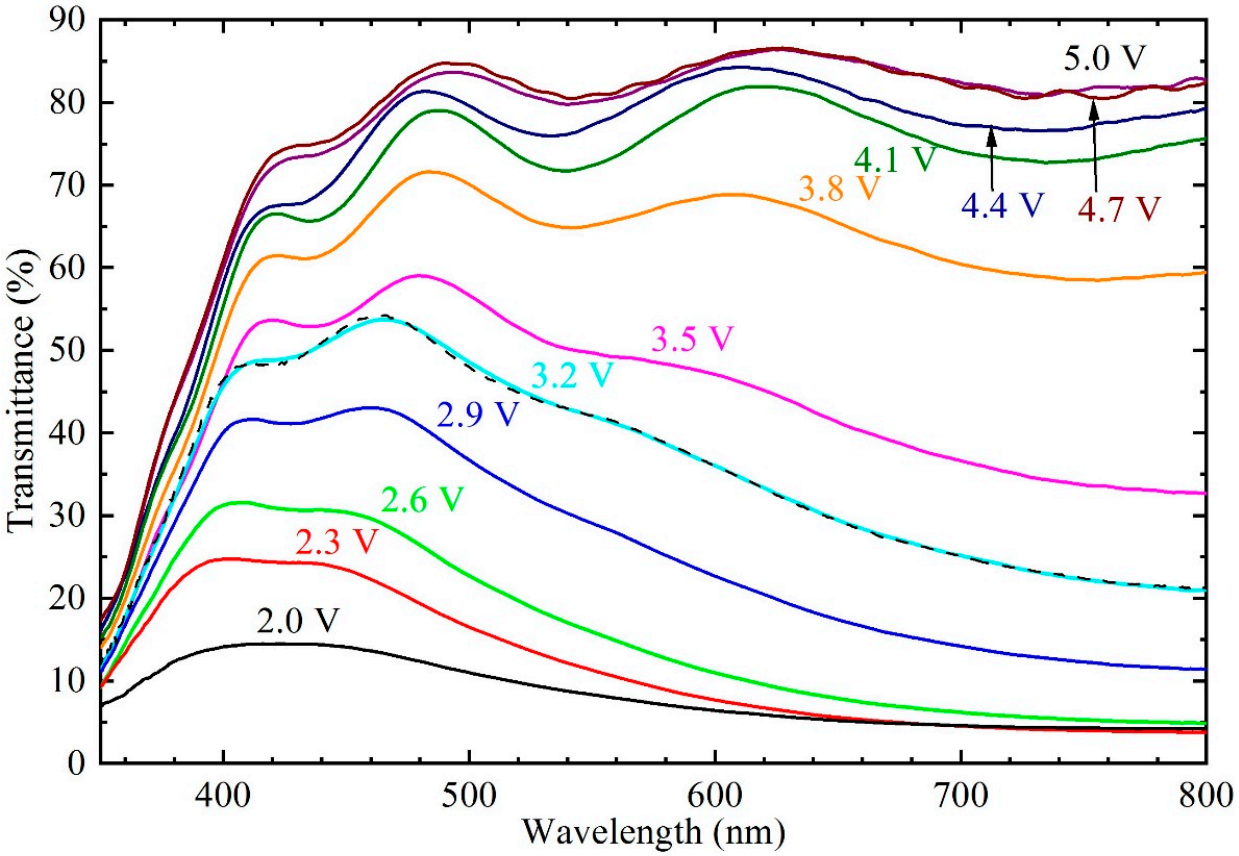

Figure 2. Spectral optical transmittance for a ~300-nm-thick film of HWO_x at applied potentials between 2.0 and 5.0 V vs. Li/Li^+. The optical transmittance of the as-deposited film is given by the dashed curve.

The color of the bleached and dark states was quantitatively assessed by calculating the CIE chromaticity coordinates (x,y,z) from the optical spectra, using the CIE 1931 Colorimetric System and the daylight illuminant D65 [42]. The bleached state is characterized by x = 0.32, y = 0.34, and z = 0.34, which signifies an almost neutral color. The dark state was found to exhibit the color coordinates x = 0.25, y = 0.28, and z = 0.47; this signifies a blue color close to that found in a previous study of hydrous WO_3 films [7].

It should be noted that complete bleaching requires potentials close to 5 V vs. Li/Li^+, which is the main difference from the behavior of non-hydrous amorphous WO_3 films. In fact, many previous studies have shown that non-hydrous WO_3 films require only 3.5 to 4 V vs. Li/Li^+ to bleach completely [7,8].

Corresponding impedance response data are given in a complex impedance plot at low potentials in Figure 3a,b and at high potentials in Figure 3c,d. The impedance varies as a function of frequency over orders of magnitude, and therefore each spectrum is plotted in two graphs so as to show all pertinent features. It is observed that higher applied potentials gave larger impedance values. It is also seen that the fits to the equivalent circuits in Figure 1 demonstrated reasonably good agreement and generally the WSSQ deviation (see Tables A1 and A2 in Appendix A) was in the range 0.01–0.1, except for potentials at 4.4 V vs. Li/Li^+ and above where it was difficult to find a good fit at the lowest frequencies as evident from Figure 3d. The quality of the fit at low potentials was mostly of the same order of magnitude as in earlier work on WO_3 [22]; however, it was difficult to obtain an accurate fit at high frequencies for some potentials, as apparent in Figure 3a. The visible high-frequency feature in the spectra is a depressed semicircle in the complex *Z*-plane; this feature is frequently overlapping with the anomalous diffusion response at low potentials and with a second semicircle at high potentials. The first depressed semicircle is due to the combination of interfacial resistance and CPE elements. It can be interpreted as being due to a combination of intermediate adsorption and double-layer effects. In spectra taken

at low potentials, only part of this semicircle was reliably detected because of noise and parasitic effects occurring at frequencies above about 20 kHz. Tables A1 and A2 give values of the circuit elements obtained from the fits to the experimental EIS spectra.

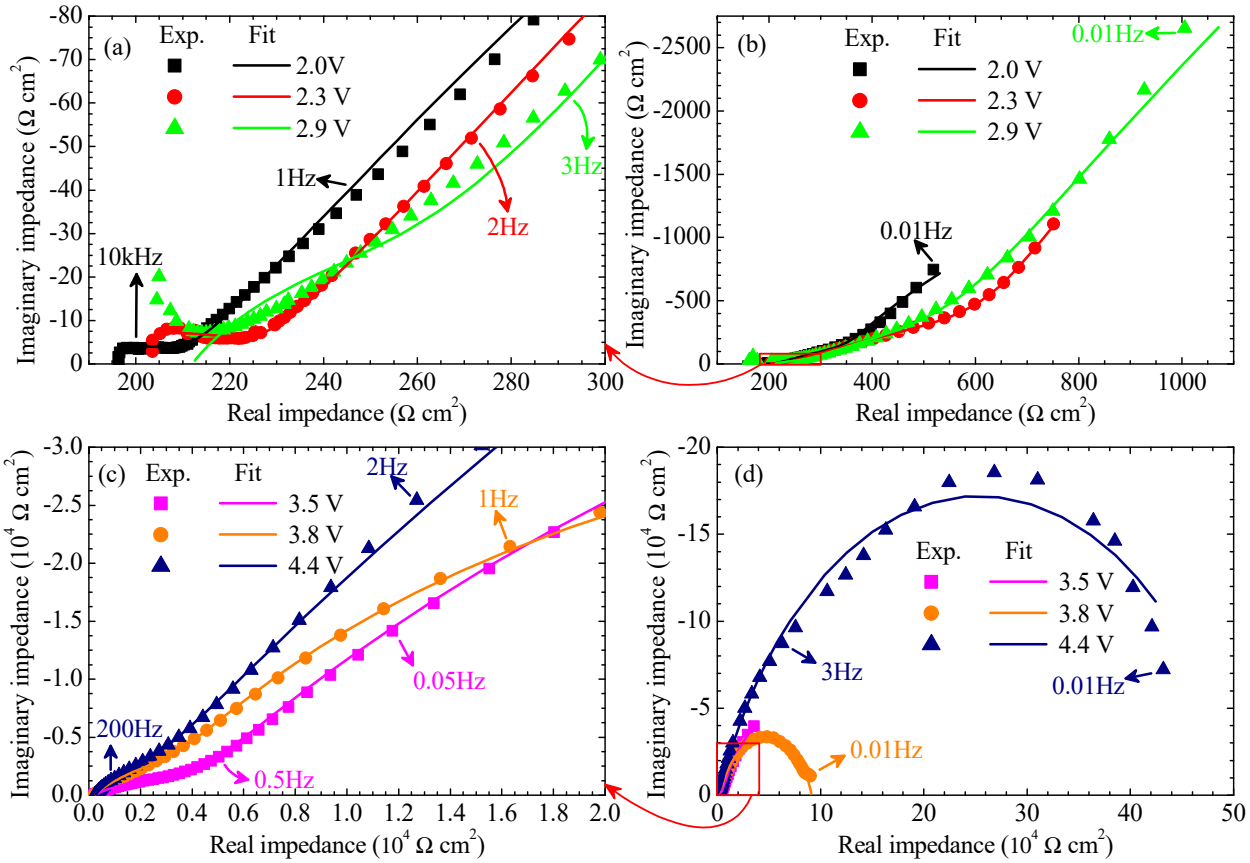

Figure 3. Real vs. imaginary impedance for a ~300-nm-thick HWO_x film measured in a Li^+-containing electrolyte: (**a**,**b**) at low potentials, and (**c**,**d**) at high potentials. Spectra were taken in the frequency range 10 mHz to 100 kHz at the shown potentials vs. Li/Li^+. Some specific frequencies are marked in the figure. Measured data are denoted by symbols and full lines represent fits to equivalent-circuit models as described in the main text.

We find that R_{ct} is of the order of 30 to 210 Ω at low potentials and abruptly increases to a few thousand ohms at a potential of 3.5 V vs. Li/Li^+. This behavior signals that the intercalation of Li ions into the film becomes considerably more difficult at potentials above 3.5 V vs. Li/Li^+. It is not possible to interpret CPE_{int} in terms of purely capacitive effects because of the frequency dependence inherent in the CPE behavior. However, τ_q, which should be proportional to an "effective" capacitance, decreases from the 10^{-4} to the 10^{-6} F-range between 3 and 4 V vs. Li/Li^+. The lower part of this range contains typical values of double-layer capacitance, while values of adsorption capacitance for non-hydrous WO_3 films were found to be of the order of mF [23]. Hence, we assume that CPE_{int} and R_{ct} have contributions from both the charging of the double-layer and the intermediate adsorption step. These two processes are probably overlapping so that they cannot be distinguished in the present case. The anomalous diffusion parameters in Table A1 are broadly consistent with previous data for non-hydrous WO_3 films [23], with some quantitative differences that are better discussed in terms of the diffusion coefficient, as we proceed to do below.

The interpretation of the data at potentials above 3.5 V vs. Li/Li^+ is more complicated. An anomalous diffusion contribution due to ion diffusion in the HWO_x film could not be resolved, but still the samples exhibited significant coloration in this potential range, as seen in Figure 2. However, it was recently shown that the intermediate adsorption process leads to coloration, in addition to the ion diffusion process [23]. Therefore, we

conclude that the adsorption process must be an important contribution to the EIS spectra at potentials above 3.5 V vs. Li/Li^+, but whether it contributes to the high-frequency or the low-frequency semicircles in Figure 3c,d is not clear. We tentatively assign the elements CPE_{int} and R_{ct} in Figure 1b to the double-layer and assume that the adsorption process is the main contribution to the low-frequency resistance and CPE. As mentioned above, chemical reactions also give rise to semicircles in the complex impedance plane, and these may affect the EIS spectra at least at the highest potentials. For example, it is known that the oxidation of propylene carbonate starts around 4.5 V vs. Li/Li^+ [43]. It is also possible that the capacitive behavior at the highest potentials was affected by the geometric capacitance of the HWO_x thin film.

We now turn to the analysis of the anomalous diffusion element Z_d. Its fitting parameters are given in Table A1 and will be discussed in terms of the chemical capacitance and diffusion coefficient, which have clear physical meanings. The chemical capacitance is the asymptotic low-frequency capacitance of the anomalous diffusion response and can, in principle, be obtained from the fit parameter c. It is also illustrative to plot the data in the complex capacitance plane via the transformation $C = 1/i\omega Z$. The curves in the complex C plane are arc-shaped and exhibit different size at each applied potential, as seen in Figure 4. The data were fitted to a semicircle and extrapolated to obtain the intercept with the real axis in order to obtain C_{chem}. This procedure works very well for potentials below 3.5 V vs. Li/Li^+, and the graphical extrapolation matched accurately with the circuit fitting. However, at higher potentials the curves bend upwards in the capacitance plane because of the influence of the low-frequency resistance R_{lf}. This quantity exhibits values of the order of a few times 10^5 Ω, as can be seen in Table A2, and could be influenced by the reaction resistance of parasitic side reactions. For these high potentials, C_{chem} values were estimated from the measured capacitance at the lowest frequencies.

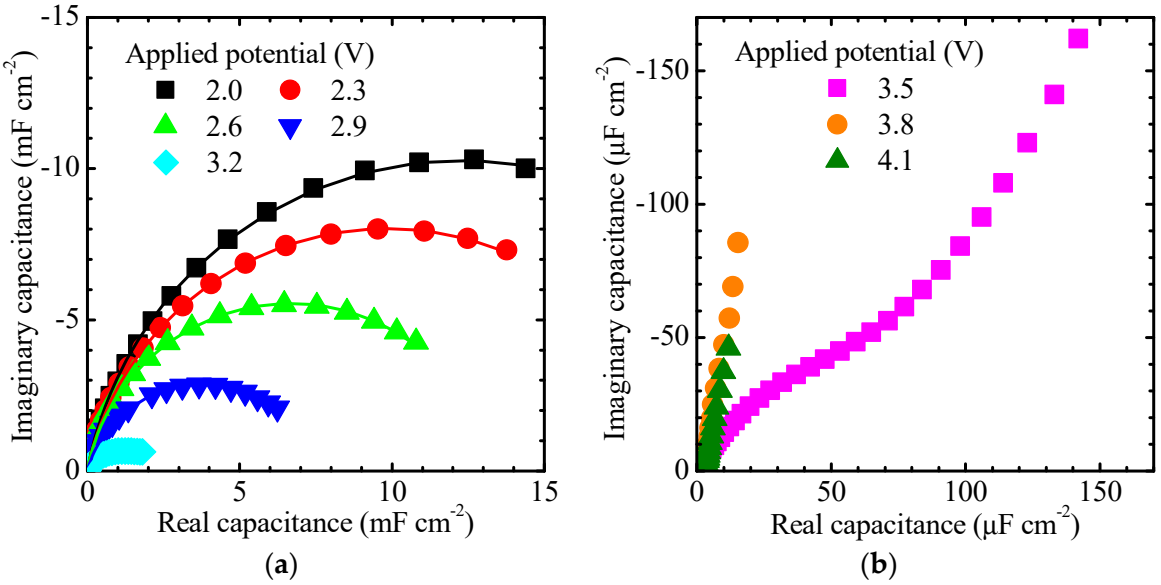

Figure 4. Imaginary capacitance vs. real capacitance for a ~300-nm-thick HWO_x film measured in a Li^+-containing electrolyte: (**a**) at low potentials; (**b**) at high potentials. Spectra were measured in the frequency range 10 mHz to 100 kHz at the shown potentials vs. Li/Li^+. Symbols indicate measured data and solid lines show the semicircle fit.

The applied-potential-dependence of C_{chem} and D were also analyzed and will be considered next. Values of C_{chem} were obtained from Figure 4 and were converted to charge capacity, dz/dU, by Equations (4) and (5). Figure 5 shows this quantity—i.e., how many ions (and electrons) per host atom are inserted in the film when the energy is changed—as a function of applied potential. It is seen that dz/dU exhibited a maximum when the film was in its darkest state and decreases smoothly when the potential was increased upon

going toward the bleached state. The maximum number of Li^+/W at the lowest potential was found to be of the order of 0.3.

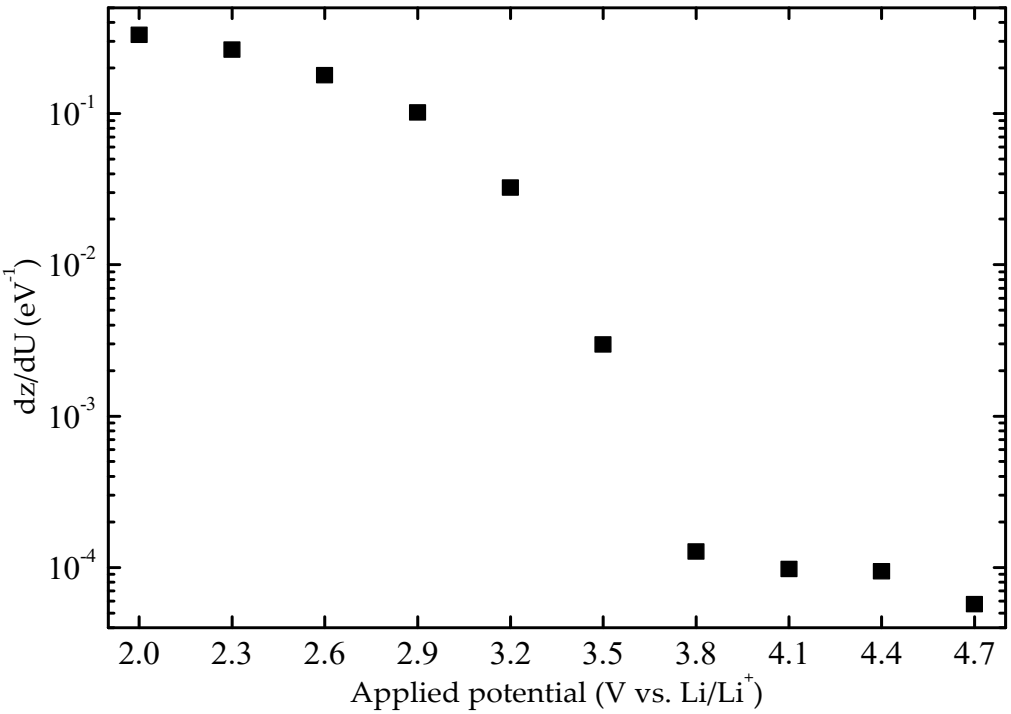

Figure 5. Charge capacity of inserted Li ions/electrons per unit potential and formula unit, denoted *dz/dU*, as a function of potential vs. Li/Li^+ for a ~300-nm-thick HWO_x film measured in a Li^+-containing electrolyte.

It has been shown that *dz/dU* can be interpreted qualitatively in terms of the electronic density of states of the material [35]. In connection with Figure 5, it has to be realized that lower potentials are equivalent to higher energies. The increase of *dz/dU* for potentials below 3.8 V vs. Li/Li^+ is qualitatively similar to the density of states of the conduction band edge in WO_3 [36,37]. However, we also observe a tail of states at high potentials, and from Figure 2 it is clearly seen that the EC behavior extends into this range. We therefore interpret *dz/dU* for potentials above 3.5 V vs. Li/Li^+ as being due to a band tail of localized states, probably associated with interfacial regions of the oxide film and with hydrogen doping introduced during thin-film deposition.

The effective diffusion coefficient was obtained from equivalent-circuit analysis of the EIS data according to Equation (3); data are reported in Figure 6. Values are slightly lower at 2.0 and 2.3 V vs. Li/Li^+ than at higher potentials. The number of Li ions in the film is largest in the dark state at low potentials. Hence, many ion sites of the film are then occupied, and therefore the ion diffusion is restricted. At higher potentials, there are more unoccupied sites, and the diffusion coefficient is expected to be larger. Data in Figure 4 are consistent with this argument. However, the origin of the detailed potential dependence is unknown; we note that a similar dependence has been observed before for non-hydrous WO_3 films [11]. The magnitude of the diffusion coefficient is in the range encompassed in our previous study of amorphous non-hydrous WO_3 films [22] although significantly lower than the highest values previously reported [22,23].

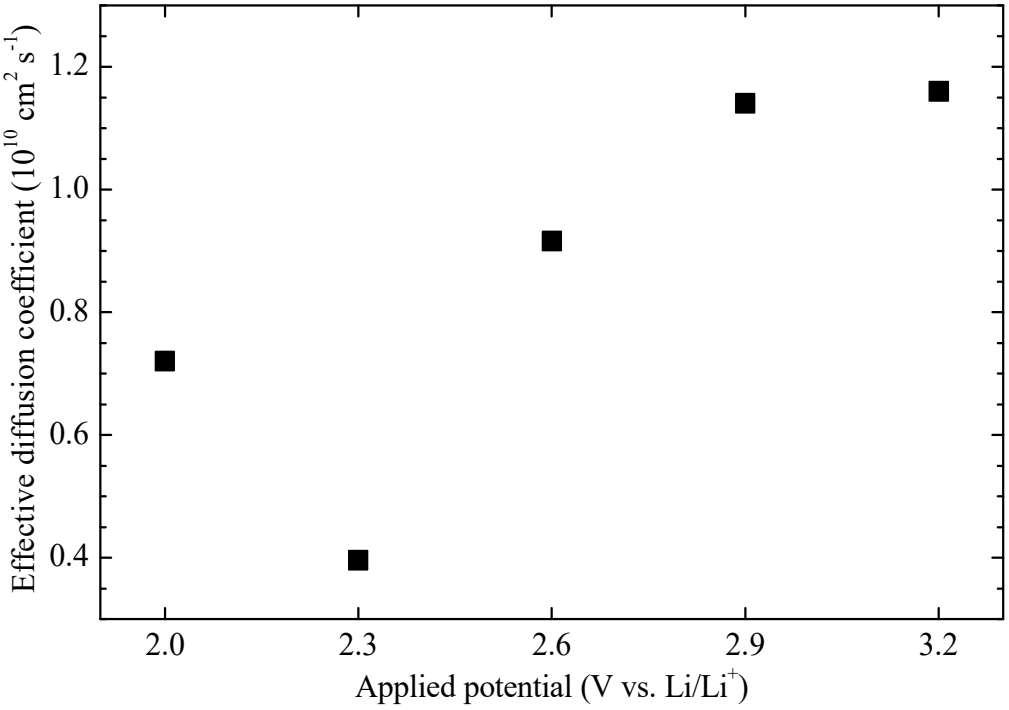

Figure 6. Effective diffusion coefficient of Li^+ ions as a function of potential vs. Li/Li^+ for ~300-nm-thick HWO_x films.

5. Conclusions

Tungsten-oxide-based films can be deposited in colored state by sputtering in a hydrogen-containing gas ambient. This fact enables the production of electrochromic devices comprising dark hydrous tungsten oxide (HWO_x) films and dark nickel oxide (NiO_y) films positioned between transparent electrical contacts and separated by an electrolyte. This production route is of considerable interest.

In the present work, we studied the optical and electrochemical properties of HWO_x films. Their electrochromic behavior as well as their impedance spectra were qualitatively similar to those of conventional non-hydrous WO_3 films. Impedance spectroscopy at potentials below 3.5 V vs. Li/Li^+ could be fitted by well-established anomalous-diffusion models. At higher potentials, a simpler equivalent circuit—which, however, is more difficult to interpret—gave a satisfactory fit to impedance spectra. Charge capacities and coloration efficiencies were similar to values for non-hydrous WO_3. The diffusion coefficients were comparable, but the values for HWO_x were found in the lower part of the range for differently prepared WO_3 films. However, the hydrous films did not bleach completely until a very high potential, of the order of 5 V vs. Li/Li^+, was applied. It seems that this effect is related to the existence of a significant band-tail, possibly due to hydrogen-related states, extending in a significant range below the conduction band edge. The large potential span embraced by the coloration/bleaching process might be an important disadvantage when it comes to applications in electrochromic devices for smart windows; this is so because parasitic chemical side reactions might be present at potentials significantly above 4 V vs. Li/Li^+. Therefore, durability issues should be given high priority in future investigations of electrochromic devices embodying HWO_x thin films.

Author Contributions: Conceptualization, E.P., C.G.G. and G.A.N.; formal analysis, E.P. and G.A.N.; investigation, E.P.; writing—original draft preparation, E.P.; writing—review and editing, C.G.G. and G.A.N.; project administration, C.G.G. and G.A.N.; funding acquisition, C.G.G. and G.A.N. All authors have read and agreed to the published version of the manuscript.

Funding: We gratefully acknowledge financial support from the Swedish Research Council, grant no. 2016-03713 and from the Swedish Research Council for Environment, Agricultural Sciences and Spatial Planning (FORMAS 2008-1352-10666-36).

Data Availability Statement: The data presented in this study are available on request from the corresponding author.

Conflicts of Interest: The authors declare no conflict of interest. The funders had no role in the design of the study; in the collection, analyses, or interpretation of data; in the writing of the manuscript, or in the decision to publish the results.

Appendix A

Table A1. Parameters obtained from fitting of experimental EIS spectra shown in Figure 3a,b and Figure 4a to the equivalent circuit depicted in Figure 1a. In addition, the weighted sum of squares (WSSQ) value of each fit is presented. Resistance and capacitance values were normalized to 1 cm^2 of electrode area.

Bias Potential (V vs. Li/Li^+)	R_{hf} (Ω)	τ_{int} (μF $s^{-1+n_{int}}$)	n_{int}	R_{ct} (Ω)	τ_q (μF s^{-1+n_q} m)	n_q	c (F m^{-1})	WSSQ
3.2	220	315	0.611	210	0.86×10^{-4}	0.242	4667	0.043
2.9	212	571	0.603	76.2	2.56×10^{-4}	0.202	14,670	0.098
2.6	184	11.8	0.598	46.1	3.66×10^{-4}	0.111	35,330	0.124
2.3	183	281	0.363	47.7	2.55×10^{-4}	0.110	45,670	0.013
2.0	186	893	0.336	28.9	6.09×10^{-4}	0.118	56,670	0.088

Table A2. Parameters obtained from fitting of experimental EIS spectra shown in Figure 3c,d and Figure 4b to the equivalent circuit depicted in Figure 1b. In addition, weighted sum of squares (WSSQ) value of each fit is presented. Resistance and capacitance values were normalized to 1 cm^2 of electrode area.

Bias Potential (V vs. Li/Li^+)	R_{hf} (Ω)	τ_{int} (μF $s^{-1+n_{int}}$)	n_{int}	R_{ct} (Ω)	τ_{lf} (μF $s^{-1+n_{lf}}$)	n_{lf}	R_{lf} (Ω)	WSSQ
4.7	249	4.88	0.753	4162	3.85	0.854	3.62×10^5	0.182
4.4	256	3.73	0.851	1635	5.16	0.762	5.04×10^5	0.174
4.1	255	4.70	0.784	2681	5.64	0.801	1.80×10^5	0.046
3.8	247	6.10	0.740	3130	7.81	0.818	0.88×10^5	0.059
3.5	230	28.9	0.562	4061	139	0.741	1.78×10^5	0.052

References

1. Granqvist, C.G. *Handbook of Inorganic Electrochromic Materials*; Elsevier: Amsterdam, The Netherlands, 1995.
2. Mortimer, R.J.; Rosseinsky, D.R.; Monk, P.M. (Eds.) *Electrochromic Materials and Devices*; Wiley-VCH: Weinheim, Germany, 2015.
3. Wu, J.W.; Chua, M.H.; Shah, K.W. (Eds.) *Electrochromic Smart Materials: Fabrication and Applications*; Royal Society of Chemistry: Cambridge, UK, 2019.
4. Lampert, C.M. Chromogenic smart materials. *Mater. Today* **2004**, *7*, 29–35. [CrossRef]
5. Granqvist, C.G. Electrochromics for smart windows: Oxide-based thin films and devices. *Thin Solid Films* **2014**, *564*, 1–38. [CrossRef]
6. Granqvist, C.G.; Arvizu, M.A.; Bayrak Pehlivan, İ.; Qu, H.-Y.; Wen, R.-T. Electrochromic materials and devices for energy efficiency and human comfort in buildings: A critical review. *Electrochim. Acta* **2018**, *259*, 1170–1182. [CrossRef]
7. Niklasson, G.A.; Granqvist, C.G. Electrochromics for smart windows: Thin films of tungsten oxide and nickel oxide, and devices based on these. *J. Mater. Chem.* **2007**, *17*, 127–156. [CrossRef]
8. Triana, C.A.; Granqvist, C.G.; Niklasson, G.A. Electrochromism and small-polaron hopping in oxygen deficient and lithium intercalated amorphous tungsten oxide films. *J. Appl. Phys.* **2015**, *118*, 024901. [CrossRef]
9. Barsukov, Y.; Macdonald, J.R. (Eds.) *Impedance Spectroscopy*, 2nd ed.; Wiley: New York, NY, USA, 2005.
10. Orazem, M.E.; Tribollet, B. *Electrochemical Impedance Spectroscopy*; Wiley: Hoboken, NJ, USA, 2008.
11. Niklasson, G.A.; Malmgren, S.; Strømme, M. Impedance response of electrochromic materials and devices. In *Impedance Spectroscopy*, 3rd ed.; Barsukov, Y., Macdonald, J.R., Eds.; Wiley: Hoboken, NJ, USA, 2018; pp. 263–281.
12. Ho, C.; Raistrick, I.D.; Huggins, R.A. Application of A-C techniques to the study of lithium diffusion in tungsten trioxide thin films. *J. Electrochem. Soc.* **1980**, *127*, 343–350. [CrossRef]
13. Randles, J.E.B. Kinetics of rapid electrode reactions. *Disc. Faraday Soc.* **1947**, *1*, 11–19. [CrossRef]

14. Yoshiike, N.; Ayusawa, M.; Kondo, S. Electrochemical properties of WO_3 x(H_2O). III. Complex plane analysis of the film on SnO_2. *J. Electrochem. Soc.* **1984**, *131*, 2600–2605. [CrossRef]
15. Bohnke, C.; Bohnke, O. Impedance analysis of amorphous WO_3 thin films in hydrated $LiClO_4$-propylene carbonate electrolytes. *Solid State Ion.* **1990**, *39*, 195–204. [CrossRef]
16. Wang, J.; Bell, J.M. The kinetic behaviour of ion injection in WO_3 based films produced by sputter and sol–gel deposition: Part II. Diffusion coefficients. *Sol. Energy Mater. Sol. Cells* **1999**, *58*, 411–429. [CrossRef]
17. Strømme Mattsson, M. Li insertion into WO_3: Introduction of a new electrochemical analysis method and comparison with impedance spectroscopy and the galvanostatic intermittent titration technique. *Solid State Ion.* **2000**, *131*, 261–273. [CrossRef]
18. Sharma, N.; Deepa, M.; Agnihotry, S.A. Impedance studies of Li inserted sol-gel derived WO_3 films. *Solid State Ion.* **2002**, *152–153*, 873–875. [CrossRef]
19. Fabregat-Santiago, F.; Garcia-Belmonte, G.; Bisquert, J.; Ferriols, N.S.; Bueno, P.R.; Longo, E.; Anton, J.S.; Castro-Garcia, S. Dynamic processes in the coloration of WO_3 by lithium insertion. *J. Electrochem. Soc.* **2001**, *148*, E302–E309. [CrossRef]
20. Bobics, L.; Sziraki, L.; Lang, G.G. The impedance related to the electrochemical hydrogen insertion into WO_3 films: On the applicability of the diffusion-trapping model. *Electrochem. Commun.* **2008**, *10*, 283–287. [CrossRef]
21. Bisquert, J.; Compte, A. Theory of the electrochemical impedance of anomalous diffusion. *J. Electroanal. Chem.* **2001**, *399*, 112–120. [CrossRef]
22. Malmgren, S.; Green, S.V.; Niklasson, G.A. Anomalous diffusion of ions in electrochromic tungsten oxide films. *Electrochim. Acta* **2017**, *247*, 252–257. [CrossRef]
23. Rojas-González, E.A.; Niklasson, G.A. Charge coloration dynamics of electrochromic amorphous tungsten oxide studied by simultaneous electrochemical and color impedance measurements. *J. Appl. Phys.* **2021**, *129*, 053103. [CrossRef]
24. Backholm, J.; Géoren, P.; Niklasson, G.A. Determination of solid phase chemical diffusion coefficient and density of states by electrochemical methods: Application to iridium oxide-based thin films. *J. Appl. Phys.* **2008**, *103*, 023702. [CrossRef]
25. Garcia-Garcia, F.J.; Gil-Rostra, J.; Yubero, F.; González-Elipe, A.R. Electrochromism in WO_x and $W_xSi_yO_z$ thin films prepared by magnetron sputtering at glancing angles. *Nanosci. Nanotechnol. Lett.* **2013**, *5*, 89–93. [CrossRef]
26. Garcia-Garcia, F.J.; Gil-Rostra, J.; Yubero, F.; Espinós, J.P.; Gonzalez-Elipe, A.R.; Chaboy, J. In Operando X-ray Absorption Spectroscopy Analysis of Structural Changes During Electrochemical Cycling of WO_3 and $W_xSi_yO_z$ Amorphous Electrochromic Thin Film Cathodes. *J. Phys. Chem. C* **2015**, *119*, 644–652. [CrossRef]
27. Atak, G.; Bayrak Pehlivan, I.; Montero, J.; Granqvist, C.G.; Niklasson, G.A. Electrochromic tungsten oxide films prepared by sputtering: Optimizing cycling durability by judicious choice of deposition parameters. *Electrochim. Acta* **2021**, *367*, 137233. [CrossRef]
28. Marszalek, K. Magnetron-sputtered WO_3 films for electrochromic devices. *Thin Solid Films* **1989**, *175*, 227–233. [CrossRef]
29. Giri, A.P.; Messier, R. Physical structure and the electrochromic effect in tungsten oxide films. *Mater. Res. Soc. Symp. Proc.* **1984**, *24*, 221–227. [CrossRef]
30. Granqvist, C.G.; Avendano, E.; Azens, A. Electrochromic coatings and devices: Survey of some recent advances. *Thin Solid Films* **2003**, *442*, 201–211. [CrossRef]
31. Azens, A.; Gustavsson, G.; Karmhag, R.; Granqvist, C.G. Electrochromic devices on polymer foil. *Solid State Ion.* **2003**, *165*, 1–5. [CrossRef]
32. Wen, R.-T.; Granqvist, C.G.; Niklasson, G.A. Anodic electrochromism for energy-efficient windows: Cation/anion-based surface processes and effects of crystal facets in nickel oxide thin films. *Adv. Funct. Mater.* **2015**, *25*, 3359–3370. [CrossRef]
33. Granqvist, C.G.; Bayrak Pehlivan, İ.; Niklasson, G.A. Electrochromics on a roll: Web-coating and lamination for smart windows. *Surf. Coat. Technol.* **2018**, *336*, 133–138. [CrossRef]
34. Franceschetti, D.R.; Macdonald, J.R. Small-signal A-C response theory for electrochromic thin films. *J. Electrochem. Soc.* **1982**, *129*, 1754–1756. [CrossRef]
35. Bisquert, J. Fractional diffusion in the multiple-trapping regime and revision of the equivalence with the continuous-time random walk. *Phys. Rev. Lett.* **2003**, *91*, 010602. [CrossRef]
36. Fournier, J.; Brossard, L.; Tilquin, J.-Y.; Cote, R.; Dodelet, J.-P.; Guay, D.; Menard, H. Hydrogen evolution reaction in alkaline solution: Catalytic influence of Pt supported on graphite vs. Pt inclusions in graphite. *J. Electrochem. Soc.* **1996**, *143*, 919–926. [CrossRef]
37. *ZView for Windows*; Scribner Associates, Inc.: Southern Pines, NC, USA; Available online: https://www.scribner.com/software/68-general-electrochemistr376-zview-for-windows/ (accessed on 25 May 2021).
38. Bisquert, J. Chemical capacitance of nanostructured semiconductors: Its origin and significance for nanocomposite solar cells. *Phys. Chem. Chem. Phys.* **2003**, *5*, 5360–5364. [CrossRef]
39. Niklasson, G.A. Electrochemical measurements of the electronic density of states. *Phys. Scr.* **2015**, *90*, 094005. [CrossRef]
40. Strømme, M.; Ahuja, R.; Niklasson, G.A. New probe of the electronic structure of amorphous materials. *Phys. Rev. Lett.* **2004**, *93*, 206403. [CrossRef]
41. Niklasson, G.A.; Malmgren, S.; Green, S.; Backholm, J. Determination of electronic structure by impedance spectroscopy. *J. Non Cryst. Solids* **2010**, *356*, 705–709. [CrossRef]
42. MacAdam, D.L. *Color Measurement: Theme and Variations*; Springer: Berlin/Heidelberg, Germany, 1985.
43. Pletcher, D.; Rohan, J.F.; Ritchie, A.G. Microelectrode studies of the Lithium/Propylene Carbonate system. Part I: Electrode reactions at potentials positive to Lithium deposition. *Electrochim. Acta* **1994**, *39*, 1369–1376. [CrossRef]